ACS APPLIED MATERIALS & INTERFACES

Research Article

www.acsami.org

Patterned Biochemical Functionalization Improves Aptamer-Based Detection of Unlabeled Thrombin in a Sandwich Assay

Lotta Römhildt,[†,‡] Claudia Pahlke,[†] Felix Zörgiebel,[†,§] Hans-Georg Braun,[⊥] Jörg Opitz,[†,‡] Larysa Baraban,[†,*] and Gianaurelio Cuniberti[†,§]

[†]Institute for Materials Science and Max Bergmann Center of Biomaterials and [§]Center for Advancing Electronics Dresden, TU Dresden, 01062 Dresden, Germany

[‡]Fraunhofer Institute IZFP Dresden, 01109 Dresden, Germany

[⊥]Max Bergmann Center of Biomaterials, Leibniz Institute of Polymer Research Dresden, 01069 Dresden, Germany

Supporting Information

ABSTRACT: Here we propose a platform for the detection of unlabeled human α-thrombin down to the picomolar range in a fluorescence-based aptamer assay. In this concept, thrombin is captured between two different thrombin binding aptamers, TBA1 (15mer) and TBA2 (29mer), each labeled with a specific fluorescent dye. One aptamer is attached to the surface, the second one is in solution and recognizes surface-captured thrombin. To improve the limit of detection and the comparability of measurements, we employed and compared two approaches to pattern the chip substrate—microcontact printing of organosilanes onto bare glass slides, and controlled printing of the capture aptamer TBA1 in arrays onto functionalized glass substrates using a nanoplotter device. The parallel presence of functionalized and control areas acts as an internal reference. We demonstrate that both techniques enable the detection of thrombin concentrations in a wide range from 0.02 to 200 nM with a detection limit at 20 pM. Finally, the developed method could be transferred to any substrate to probe different targets that have two distinct possible receptors without the need for direct target labeling.

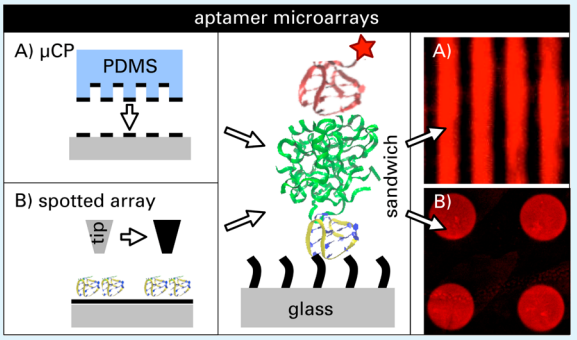

KEYWORDS: *biosensor, selective functionalization, aptamer, thrombin, sandwich assay*

INTRODUCTION

The early detection of disease markers, pathogenic cells, molecules, or drugs is a key driving force for the development of simple and rapid diagnostic techniques to assure specific and timely treatment.[1,2] Numerous efforts are nowadays directed towards miniaturization and multiplexed sensing for portable and cost-effective devices aiming at personalized diagnostics. To date, standard technologies like polymerase chain reaction (PCR) or immunoassays (e.g., ELISA) using antibodies for sensing[3] are highly specific but complex and require highly qualified employees, laboratory equipment, relatively long assay times, or a large sample volume. Recently reported DNA aptamers (i.e., oligonucleotide chains)[4−6] represent an alternative to antibodies as highly specific receptors for cost-effective biosensors. These aptasensors rely mostly on either monitoring of electrical characteristics[7−10] or optical properties of devices[11−13] and open up possibilities for real-time or label-free biosensing. Among the most frequently employed techniques, microarray technologies enable integration of several experiments on one chip for parallel detection of different analytes.[14−17] In combination with lab-on-a-chip technologies, fast and sensitive sensors can be developed.

One of the remaining challenges in the field of biological detection is related to improving the selectivity of the assay and reducing the background noise caused by unspecific adsorption.[18,19] High specificity of the whole biochemical scheme determines the detection limit of the technique. In parallel to already well-studied antibodies,[18,20] the use of engineered receptor molecules, which are more stable and can be developed at low cost, i.e., aptamers, still need to be optimized for their wider implementation into biochemical assays.[21−23] Because of its distinct sequence, each aptamer forms a tertiary structure (e.g., hairpin or quadruplex[24,25]), which interacts with a certain recognition site of the analyte such as proteins or organic molecules.[26] Easy labeling protocols or the attachment of functional end groups to the nucleotides, the higher stability under varying conditions such as temperature or ionic strength compared to antibodies as well as the wide variety of possible targets make aptamers a promising candidate for diverse biosensor applications in the future.[13,21,26,27]

Received: September 5, 2013
Accepted: October 31, 2013
Published: October 31, 2013

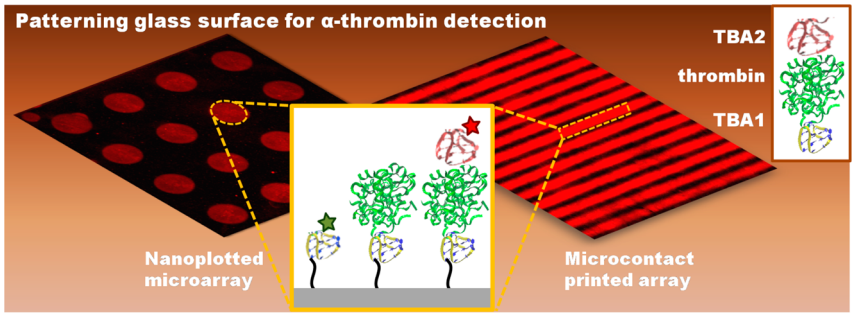

Figure 1. Conceptual visualization of the aptamer based sensing platform with fluorescently labeled aptamers (TBA1 with green and TBA2 with red label) forming a sandwich with thrombin on patterned glass surfaces, i.e., spotted microarray (left) and microcontact printed array (right). Molecular structures for this scheme were taken from the RCSB protein data bank (PDB ID: 1HAO)[39] and visualized in VMD 1.9.1.

Thrombin is a protein that exhibits enzyme- and hormone-like properties.[28] The molecule plays an important role in the blood coagulation cascade where it converts fibrinogen into fibrin for clotting, and it stimulates the process of platelet aggregation. Its role in cardiovascular diseases,[29] inflammation reactions and tissue recovery make thrombin an interesting candidate for medical related biosensing applications. Because of the stable quadruplex conformation of thrombin binding aptamers,[24] thrombin detection is also an excellent model system used to develop aptasensors on different sensor platforms such as fiber optic, bead or spotted microarrays for fluorescence detection,[14,30,31] electrical sensors based on inhibition of electron transfer upon recognition,[32] impedance sensors,[5] electrochemical nanosensors,[8] or mass-sensitive platforms.[33]Because of the availability of two distinct aptamers for thrombin, sandwich assays were also developed on various sensor techniques involving nanoparticles, beads, and quantum dots in combination with fluorescence[31,34,35] or electrochemiluminiscence[36] with detection limits down to 30 fM for an electrochemical approach on nanoporous gold.[37] Concentrations in the upper picomolar range indicate thrombin-related diseases with coagulation irregularities whereas normal levels can be found at μM down to nM range.[38] Thus, label-free and fast sensors able to measure from nanomolar down to the picomolar range are important to recognize and distinguish healthy from disease thrombin levels.

Here we present a setup for fluorescent detection of thrombin from nano- down to picomolar concentrations using aptamers as recognition elements. Firstly, we use two strategies to pattern the surfaces for bio-assaying: (i) microcontact printing (μCP) of linker molecules and (ii) direct nanoplotting of aptamers. Further, we introduce a sandwich setup which consists of two different available aptamers. By labeling the aptamers with a fluorescent dye, arrays of fluorescent stripes or spots are finally created. The direct comparison to on-chip background areas results in a highly sensitive assay with improved detection limit and high fluorescence-to-background amplification ratio (F2B) even in the picomolar range of concentrations. This allows to detect unlabeled thrombin as conceptually shown in Figure 1.

EXPERIMENTAL SECTION

Materials and Reagents. The Sylgard 184 silicone elastome kit was used for preparation of polydimethylsiloxane (PDMS) molds (VWR International GmbH). Biochemical functionalization was carried out with 3-aminopropyl-triethoxysilane, N-hydoxysuccinimid ester (NHS), N-(3-Dimethylaminopropyl)-N′-ethylcarbodiimide hydrochloride (EDC HCl), phosphate buffered saline tablets (PBS), glycine, tris(hydroxymethyl)aminomethane hydrochloride (Tris HCl) and Trizma® base (Sigma-Aldrich Inc.), succinic anhydride and bovine serum albumin (BSA) powder (Merck KGaA). PBS tablets were used to prepare a 10 mM immobilization buffer. DNA aptamer strands (Eurofinsdna) were ordered with two different TBA sequences: TBA1 (15-mer with polyT tail, 5′−GGTTGGTGTGGTTGG(T)$_6$-(CH$_2$)$_6$-NH$_2$-3′), TBA1-Fluorescein amidite (5′-FAM-GGTTGGTGTGGTTGG -(CH$_2$)$_6$-NH$_2$-3′) and TBA2-red (5′-rhodamine red-(T)$_6$-AGTCCGTGGTAGGG-CAGGTTGGGGTGACT-3′) and a control sequence (5′-CA-CACTCTGTCAACCTAC-(CH$_2$)$_6$-NH$_2$-3′). Spacers (CH$_2$)$_n$ and polyT sequences were included to separate the functional end (terminal group or fluorophore) from the actual aptamer folding region. These spacers have shown to significantly improve the aptamer based biorecognition as they reduce the influence of covalent immobilization, the aptamer structure is thus little influenced.[15,40] The human α-thrombin stock solution in a 50/50 glycerol/water mixture (Haematechnologic Technologies Inc.) was diluted in the binding buffer, which contained 10 mM Tris, 20 mM MgCl$_2$, was adjusted to pH 7.4 using 1 M NaOH and filtered through a 0.2 μm syringe filter. TGF-β1 (recombinant human transforming growth factor beta 1 from R&D Systems) was stored as a 3.91 μM stock solution at −80°C in 4 mM HCl and further diluted to 39.1 nM with Tris buffer for the control protein experiment.

Preparation of the PDMS Stamp. For preparation of PDMS stamps, standard protocols can be found elsewhere.[41−44] The PDMS stamp was glued onto a small holder, which was then used for manual printing onto planar samples.

Chemical Surface Modification. Silicon dioxide surfaces play an important role in various biosensor types (semiconductor based biosensors[45−47] or glass substrates for microarrays,.[48,49] To covalently link biological receptors to the surface, covalent surface modification with organosilanes is mostly used.[47,50] In this case, 3-aminopropyl-triethoxysilane (APTES) was chosen for terminal amines. The aptamers were provided with a terminal amino group. With the help of the crosslinker succinic anhydride, aptamers were immobilized on the APTES surface. Succinic anhydride creates carboxy groups and their activation was carried out with EDC and NHS, both zero-length crosslinkers. By this, stable amide bonds with the amino group of the aptamer formed.

Glass slides for both μCP and nanoplotting were thoroughly cleaned and oxygen plasma treated for hydroxylation directly before silanization to create silanol groups. A 1 % silane solution in absolute ethanol (v/v) was prepared. The PDMS stamp was covered for 5 min with a 25−50 μL droplet of the solution. After removing excess liquid, the stamp was blown dry for 15 s using a strong N_2 stream. The stamp was gently pressed onto the SiO_2 surface for 1 min. For surface characterization and dot arrays, the samples were prepared the following way. A glass slide was immersed in an ethanol−water solution (5 % DI water) with 2 % silane for 30 min. Silanization was followed by postbaking the samples for crosslinking and stabilization of the APTES layer for 10 min at 110 °C. After APTES attachment, the samples were incubated in a 200 mM borate buffer at pH 8. After

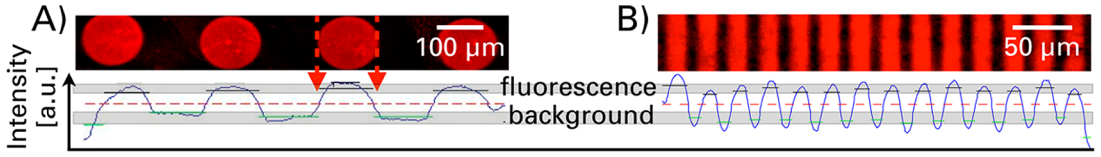

Figure 2. Schematic drawing of the automated F2B analysis of the raw image data in matlab. (A) Nanoplotted spot array. Dashed arrows indicate area dimensions for signal area. (B) Microcontact printed array. Red dashed lines indicate the threshold level between fluorescence and background signal. Solid green and black lines indicate averages of fluorescence and background levels, respectively.

the addition of succinic anhydride dissolved in DMSO (final concentration: 10 mg/mL) the amino surface was carboxylated in a ring-opening reaction. After 30 min, the samples were rinsed with DI water in an ultrasonic bath for 3 min and dried with N_2. Samples were directly processed further or stored in N_2 at 4°C until needed.

Sandwich Assay. The thrombin binding aptamers TBA1 and TBA2 bind to two distinct recognition sites of thrombin and can thus be used to realize a format of sandwich assay[17,24,51−53] as illustrated in Figure 1 (inset). The shorter aptamer TBA1 (15mer) recognizes the fibrinogen binding sites, the longer 29mer TBA2 specifically attaches to the heparin binding site.[24,54] The first aptamer labeled by fluorescein amidite (FAM - green) proves the covalent attachment of the capture aptamer (TBA1) to the substrate surface. After the injection of analyte solutions, the second aptamer (TBA2, labeled by rhodamine red) is aimed to assure the presence of the thrombin at the surface and to quantify the concentration of the molecules captured during the assay. Once the concentration of thrombin in solution changes, the resulting fluorescence signal caused by labeled TBA2 varies. Thus, the biorecognition process happens twice during the assay, which improves specificity of the method, and can lead to an increased signal and a lower detection limit. To further enhance the fluorescence-to-background amplification ratio (F2B) of the experiment and to simplify the interpretation of the results, we define the thrombin detection regions by chemically patterning glass surfaces in form of microarrays (see Figure 1).

Aptamer Coupling to the Patterned Area. To covalently attach amino-terminated TBA1, we incubated the samples in a 100 mM EDC and 50 mM NHS solution in the immobilization buffer for 10 min and rinsed with buffer and water. After blowing dry in N_2, the glass slides were immediately functionalized with the ssDNA strand. TBA1 solutions for the capture layer were freshly prepared with a concentration of 20 μM in PBS. μCP areas were covered with 25 μL of the solution and left in a wet tissue chamber for 1 h. Samples for the nanoplotter were prepared the following way. Droplets of 50−70 pL TBA1 solution were spotted onto the activated surface in small arrays. Directly after TBA1 attachment, the glass slides were transferred to sterile well plates for all further biorecognition steps of the sandwich assay. To block unreacted carboxy groups, we incubated the samples with 1 M Tris HCl, pH 7.4, followed by a rinse with the binding buffer.

Biorecognition. To show that all three components that participate in the sandwich were actively interacting with each other, i.e., to show their bioactivity in the liquid phase, we performed gel electrophoresis in native polyacrylamide gels with subsequent protein staining employing different combinations of both aptamer TBA1 and TBA2 and thrombin, see details in the Supporting Information, Figure S1, and refs 23 and 52.

To prevent unspecific protein attachment, we blocked the glass slides with a BSA solution of 0.5 mg/mL in binding buffer for 20 min. This buffer also contained 20 mM of $MgCl_2$ to promote TBA1 folding.[11] After gentle and repeated buffer rinse, the thrombin solution at various concentrations was added to react for 30 min, rinsed four times with buffer to remove unbound thrombin and incubated with 200 nM labeled TBA2 solution for 30 min to visualize the biorecognition of thrombin by immobilized TBA1. This last step was followed by buffer rinse, water rinse to remove buffer residues, and gentle N_2 blow to dry the samples prior to imaging. Optimization of the concentrations of each layer (TBA1, thrombin range, TBA2 with red dye) was carried out according to literature[14,17,51] and own initial experiments. Here, 20 μM instead of 2 μM TBA1 resulted in a higher fluorescence intensity (see Figure S2 in the Supporting Information), which is important for improving the detection limit. Tests with the quartz crystal microbalance with dissipation monitoring (QCM-D) showed a signal saturation after injection of 200 nM thrombin (see Figure S3 in the Supporting Information). Higher concentration of 1 μM thrombin led to marginal signal changes, which indicates an upper detection limit.

Data Analysis of Fluorescence Images. Images were acquired with a Zeiss Axiovert 200 microscope and Zeiss filterset 10 (emission at 515−565 nm, green) and 15 (emission at 590 nm, red), respectively for FAM and rhodamine red dyes. The microscope settings were kept constant during all measurements. For the concentration measurements the exposure time for TBA2-red was set to 1 s giving sufficient intensity for the investigated range of thrombin concentrations. The collected raw data was automatically flattened by point-wise division with a fourier transform based low-pass filter with a hard cutoff-frequency at 3 over image width that was implemented in a matlab (Mathworks, Inc. MA, USA) script. The local background signal in passivated areas (background B) and the fluorescence signal in functionalized detection areas (fluorescence F) of the flattened image were then determined for each stripe or circular spot, finally resulting in a fluorescence intensity amplification ratio (F2B). It is important to note that flattened images as well as the final signal F2B are calculated as ratios of intensity data, which makes data comparable among experiments with different illumination conditions because of lamp intensity fluctuations and adjustment variations. For largely unbiased analysis, threshold values between dark and bright image areas were automatically determined using the matlab script. Fluorescence and background intensities were averaged for each spot, as shown in Figure 2. For each concentration of the nanoplotted samples, 7 different areas (each with 4 spots) per concentration were analyzed row by row as presented in Figure 2A. Although this method includes the dark corners because of the circular signal area, their effect on the F2B value is small and thus accepted in favor of a fast analysis. Figure 2B illustrates the automated analysis of the stripe samples that do not suffer the mentioned circular image area problem. Each image delivers 14 F2B values. For each concentration, 3 images were averaged.

RESULTS AND DISCUSSION

Functionalization and Patterning. We apply (i) microcontact printing (μCP) of organosilanes or (ii) nanoplotting of TBA1 on carboxy surfaces, see Figure 1. One of the advantages of patterning is that the printed surfaces always provide control areas without functionalization. This helps to detect unspecific adsorption and background signal levels and allows to acquire better statistics with low liquid sample amounts. For the purposes of our experiment, 3-aminopropyl-triethoxysilane (APTES) was chosen for terminal amines. The aptamers were provided with amino groups. With the help of the crosslinker succinic anhydride, aptamers were immobilized on the APTES surface. The detailed procedure on modification of the glass surface is described in the Experimental Section. Further, we followed two different procedures to prepare patterned substrates for biochemical thrombin detection. In the case of microcontact printing (μCP),[41,44] the silanization step on glass was carried out by direct printing of the PDMS stamp,

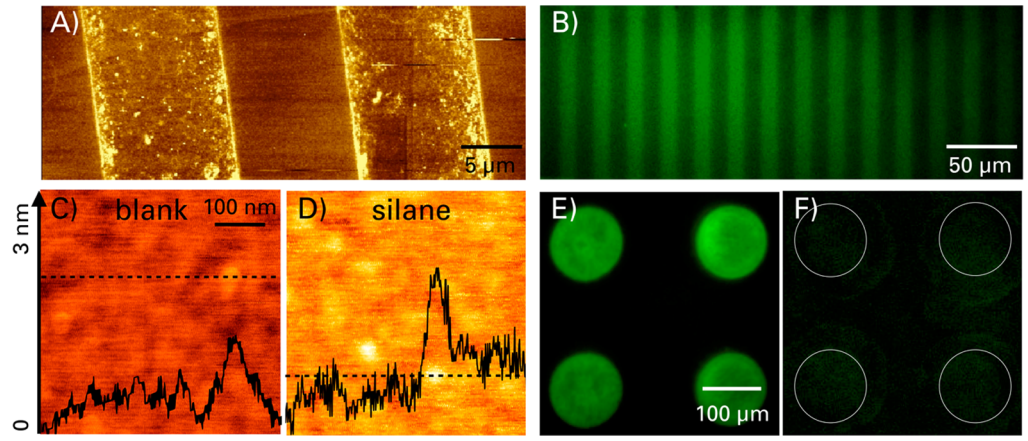

Figure 3. (A) AFAM topography image with z = 1.6 nm (dark = 0.0 nm). Microcontact printed APTES stripes appear brighter than the clean flat non-functionalized area in between. Stripe height indicates presence of a silane monolayer with partially thicker parts especially at the stamp edges (double layer). (B) TBA1 specifically binds to printed silane areas. (C) AFM topography image of a clean wafer with SiO_2 surface, z = 3 nm. (D) AFM topography image of a planar APTES-modified surface with higher roughness, z = 3 nm. (E) Nanoplotted TBA1 spots after rinsing. (F) Control: nanoplotted TBA1 spots after rinsing without carboxy group activation via EDC/NHS. White circles indicate the extents of fluorescent areas in E.

covered with a thin layer of functional molecules similar to previous works.[43,55−58] By this, silanes can be attached to the surface forming large scale regular patterns. In the second case, TBA1 solutions were spotted onto activated glass slides using a nanoplotter device (GeSiM mbH). The picoliter pipette programmably forms arrays of droplets containing 50−70 pL sample solution. This results in arrays of spots (here 20 × 20) with individual spot diameters of around 100 μm on the carboxylated surface. The array dimension can be easily enlarged with the nanoplotter.

To verify the attachment and study the quality of the stamped organosilane, we used atomic force acoustic microscopy (AFAM). Because of the detection of the acoustic amplitude signal which allows us to distinguish different levels of softness of surface layers, it is possible to evaluate the layer quality.[59] The printed stripes on a Si wafer 100 with native oxide (Figure 3A) show a homogeneous layer and monolayer quality except for the edges of the stamp stripes were silane solution can concentrate during printing because of the applied pressure. Therefore, careful drying of the incubated stamps is necessary for homogeneous monolayers. The blank control area in between the printed areas, however, appears clean and flat. Contamination with silane molecules of the blank areas for octadecyltrichlorosilane[55] could not be observed to such an extent, which assures a real difference between printed and blank area. As APTES is a short molecule, layer thickness is thin and self-assembled monolayer (SAM) formation ability is restricted compared to SAMs originating from molecules with longer chains.[19]

The chemical functionalization steps of planar glass surfaces prepared for further nanoplotting experiments were analyzed using atomic force microscopy (AFM), ellipsometry, contact angle measurements. Zeta-potential was measured with functionalized silicon nanowires in solution and APTES binding could be confirmed with Fourier transform infrared spectroscopy with attenuated total reflectance (ATR-FTIR).

The layer thickness of the covalently attached APTES was determined with a laser ellipsometer (SE 400 from SENTECH) on functionalized silicon 100 wafers with native oxide. As an approximation, the refractive index of SiO_2 of 1.4572 was used for APTES and succinic anhydride as well.[60] With a mean native oxide thickness of 2.0 nm, the functionalization layer thickness could be determined to range from 0.7-1.0 nm which corresponds well with the maximum theoretical monolayer thickness of attached and vertically aligned APTES molecules of 0.7 nm. Longer incubation times led to an increased thickness, indicating more than one monolayer. Carboxylation was proven the same way resulting in a further layer thickness increase to 0.9−1.1 nm, which is also in good agreement with the maximum theoretical thickness of 1.2 nm. Dealing with silanes, one has to consider hydrolysis and polymerization in solution as well as noncovalent interactions leading to molecule stacking and irregular layers.[19] For some biosensing applications, it might be more important to have full surface coverage to prevent unspecific adsorption, which can be assured with higher adsorption times than a perfectly ordered self-assembled monolayer.

Bare SiO_2, APTES attachment, and carboxylation can be well-distinguished with static contact angle measurements with the sessile drop method using water droplets of 1.5 μL volume. Depending on the incubation time, we could measure a mean contact angle of 63° for APTES, compared to below 10° for freshly plasma etched glass slides in good agreement with earlier reported values.[61] The success of carboxylation was indicated by a significant decrease in the contact angle down to 36°. Comparing the surface topography using an atomic force microscope (AFM) in Figure 3D to the blank sample (Figure 3C) demonstrates the roughness and height increase after silane attachment.

Zeta-potential measurements of functionalized silicon nanowires with native oxide shell after plasma activation, APTES and succinic anhydride attachment confirm the modification procedure. For details of the experimental setup, we refer to the description and Figure S4 in the Supporting Information. Hydroxy and carboxy groups possess a distinct negative zeta-potential (−32.99 and −30.07 mV), whereas the protonated amines exhibit a positive surface charge (+23.2 mV). APTES binding was verified using infrared spectroscopy (ATR-FTIR) on Si wafer crystals with native oxide surface. The spectrum in transmission (see Figure S5 in the Supporting Information) testifies the NH_2 bending and the CH_2 stretching at the

frequency ranges which are characteristic for APTES as shown by Lapin et al.[62]

Thrombin Detection. During the incubation of μCP slides in aptamer solution, TBA1 with fluorescence label for confirmation of the binding strategy was attached covalently. Only the areas of the printed stripes appeared green, proving selective attachment (see Figure 3B). The control area in between shows little unspecific adsorption. Nanoplotting of fluorescent TBA1 onto activated carboxy-terminated surfaces also led to a pattern of TBA1 attachment areas and confirmed the surface functionalization (Figure 3E). The functionalization procedure to attach TBA1 as a capture layer for thrombin was additionally tested by leaving out the step of carboxy group activation as a control. Without EDC/NHS, almost no fluorescence was observed, see Figure 3F) for spotted aptamer solution. This shows that only little unspecific adsorption of the DNA is happening and that carboxy modification and the activation were successful. Further detection of thrombin and TBA2 with a fluorescent red label proves the activity of immobilized TBA1 and is presented in Figure 4.

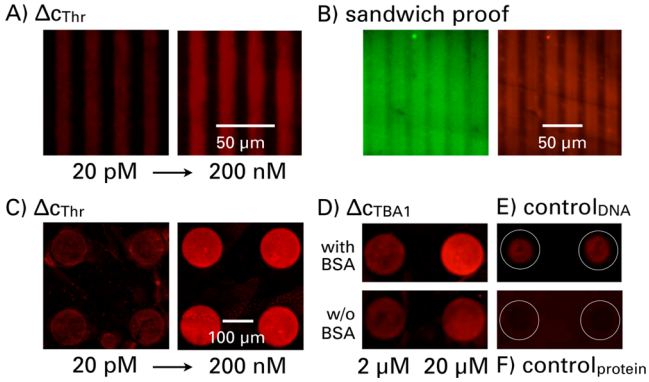

Figure 4. Fluorescence images of thrombin concentrations 20 pM and 200 nM at fixed TBA1 and TBA2 concentrations on (A) μCP and (C) nanoplotted samples. (B) Proof of sandwich assay. The bright dot is an artefact but allows to confirm labeling of the same region with TBA1-green and then TBA2-red after thrombin detection. (D) Spots with two different TBA1 concentrations, 2 and 20 μM, are plotted. Without BSA blocking (lower image), the F2B value of each spot is reduced compared to the sample with BSA (upper image). All other conditions were the same. (E) Control aptamer instead of TBA1 as capture layer results in irregular shaped dots clearly distinguishable from the samples with homogeneous spots and intensity distribution. White circles indicate the extents of fluorescent areas in samples with TBA1 as capture aptamer. (F) Protein control (TGF-β) to confirm selective attachment of thrombin and TBA2 to the spot area.

Applying the sandwich assay to a μCP surface using TBA1 and TBA2, each with fluorophore (see Figure 4B), shows that the same region is labeled in green (Figure 4B, left) and red (Figure 4B, right) proving the specificity of the detection. To detect the green fluorescence, longer imaging of 3 s was required. Here, the fluorescence also appears more blurry than in Figure 3. This is due to the sequence of incubation steps for blocking and biorecognition after attachment of TBA1-green.

Several slides with μCP areas or nanoplotted TBA1 were incubated with different thrombin concentrations ranging from 20 pM to 200 nM (μCP, 20 pM−2 nM−200 nM; spot array, 20 pM−2 nM−50 nM−60 nM−100 nM−150 nM−200 nM), labeled with 200 nM TBA2-red and analyzed. Panels A and C in Figure 4 exemplarily display the results for 2 concentrations for both patterning routes −20 pM and 200 nM. In both case,s a clear signal for low thrombin concentrations is detectable. The effect of blocking was tested for the nanoplotted samples (see Figure 4D). Two dots with 2 μM (left) and 20 μM (right) capture layer TBA1 are presented with (upper row) and without (lower row) BSA. Thrombin and TBA2 are both kept constant at each 200 nM. Without BSA blocking, more thrombin can simply physisorb to the surface parts without TBA1 layer and this results in a lower fluorescence amplification ratio (F2B). In the case of 20 μM TBA1, the F2B value is 1.17 with BSA and only 1.10 without BSA. This indicates a successful blocking method enhancing the contrast and improving the detection limit. We replaced the immobilized receptor with a single-stranded control DNA (Figure 4E). This results in blurry and irregular shaped spots distinct from those arrays with TBA1 as capture layer. As a second control, the protein TGF-β1 was introduced instead of thrombin (Figure 4F). The spot area, indicated by the white circle lines, appears even darker than the surrounding background area. We attribute this to the higher negative charge of the spot area because of the bound DNA, which repels the approaching TBA2. For the calibration curve, nanoplotted arrays were analyzed using an analysis method implemented in matlab program, which extracts the F2B ratios as described earlier (Figure 2).

The calibration curve for nanoplotted samples is depicted in Figure 5 (red circular symbols) in logscale. At subnanomolar

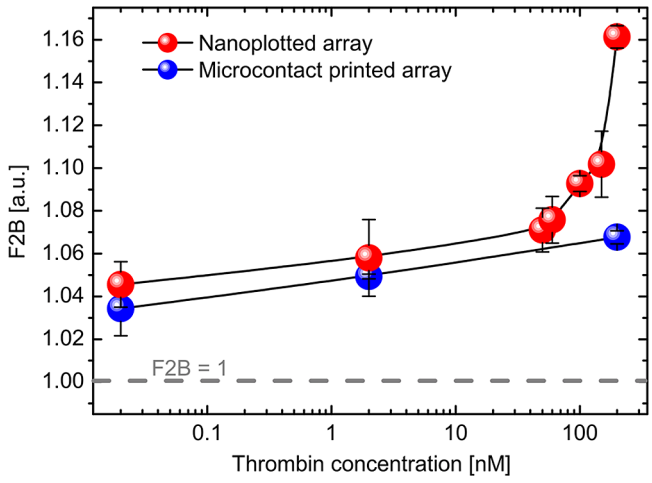

Figure 5. Fluorescence-to-background amplification ratios as a function of the thrombin concentration ranging from 20 pM to 200 nM at fixed TBA1 and TBA2 concentrations for nanoplotted (red circles) and microcontact printed (blue circles) arrays.

concentrations, the fluorescence amplification ratio increase is small compared to the steep slope until 200 nM. Here, the curve is presumably approaching the saturation level for a 20 μM capture layer of TBA1 which is consistent with optical thrombin detection presented by Cho et al.[14] using Cy3-labeled thrombin and our results using QCM-D technique (see the Supporting Information, Figure S3). This means that higher levels cannot be distinguished anymore. From the result presented in Figure S2 in the Supporting Information, probing two different capture layer concentrations, we thus conclude that the detection range can be further tuned in certain limits by varying the TBA1 concentration spotted on the surface. A lower capture layer density might thus be helpful to detect

higher thrombin levels than 200 nM. Concerning the lower limit of thrombin concentrations with the here presented setup, detection of thrombin levels in the subnanomolar range at 20 pM is possible. A fluorescence biosensor with sandwich assay based on gold nanoparticles could achieve detection limits even down to 0.43 pM.[63] However, our approach shows an improved detection limit compared to Meneghello et al., who recently reported a limit of 250 pM in a similar assay,[17] and the clear signals in our case may allow for detection of even lower concentrations. Other optical techniques such as fluorescence or electrochemiluminiscence involving quantum dots or beads in combination with sandwich assays reached limits in the hundreds of pM range[35] up to nM values.[34,36] Meneghello et al. and Zhao et al. tested their sandwich assays (fluorescence microarray and gold nanoparticles, respectively) in a serum spiked with thrombin and could show a decrease in their detection yield at lower serum dilutions.[17,64] When diluting the serum at least 5−10×, its influence was small to negligible. We admit that our approach might undergo a similar degradation in pure serum, but this can be overcome by diluting it at this reasonable ratio.

The μCP samples were equally analyzed for three protein concentrations and the F2B also increases from 20 pM to 200 nM (blue circles in Figure 5) but the slope of the curve is less steep than for the nanoplotted samples. This might be due to the small stripe width and possible silane diffusion onto the reference areas during printing. As the printing was carried out manually, sample-to-sample variations due to an irregular applied pressure and silane diffusion may have occurred. Microcontact printed arrays show an equal sensitivity for low thrombin concentrations compared to the spotted microarray.

We developed a variety of tools to confirm each functionalization step for general aptasensor development with silicon dioxide surfaces, like glass slides or silicon-based electronic sensing devices. With our approach, on-chip referencing of different modification steps and a twofold biorecognition allow for high specificity of the assay. It is, however, limited by the availability of either two distinct receptors or two binding sites present on the analyte surface.

CONCLUSION

We demonstrate a fast, simple, and low-cost detection of thrombin down to the picomolar concentration range relevant for disease diagnosis, i.e., coagulation irregularities. By combining a sandwich assay of two distinct DNA aptamers, TBA1 and TBA2, human α-thrombin was detected in a fluorescence based biosensing method with two different patterning techniques, namely μCP and nanoplotting to distinguish between control and modified surface areas. We showed a set of experiments to proof each step of binding, the effect of unspecific adsorption and the importance of blocking to achieve detectable signals even for low analyte concentrations. Both patterning routes, μCP of silanes and nanoplotting of the capture layer, lead to microarrays with high and comparable sensitivity for thrombin detection in this sandwich. Finally, we present that by optimizing each step in the sandwich assay one can tune the detection range of the unlabeled protein down to the pM range. The advantage of μCP technique is that patterns can be created starting with the first modification step, which allows for control of each functionalization step. Nanoplotted arrays show a better fluorescence amplification ratio as the risk of contaminations of the background area during the patterning step is lower. The aptamer sandwich setup only gives a positive signal after dual biorecognition with both aptamers and acts as reference for the development of novel aptasensors based on electrical[8,65] or optical transducers.[11,13] An advantage of this developed biodetection format will be the possibility to test real samples more easily since no target labeling is required for sensing. The actual biorecognition of thrombin and TB2 on TBA1-functionalized glass slides requires a reaction time of only 1.5 h in total before imaging assuring rapid biosensing with this method. Finally, the developed method can be enlarged to fast and cheap microarray techniques.

ASSOCIATED CONTENT

Supporting Information

Additional characterizations (electromobility shift assay), optimization of concentration for sandwich setup tuning capture layer concentration, testing the upper thrombin concentration limit with a quartz-crystal microbalance, as well as additional techniques to confirm the chemical fucntionalization. This material is available free of charge via the Internet at http://pubs.acs.org.

AUTHOR INFORMATION

Corresponding Author

*E-mail: larysa.baraban@nano.tu-dresden.de.

Author Contributions

The manuscript was written through contributions of all authors. All authors have given approval to the final version of the manuscript.

Notes

The authors declare no competing financial interest.

ACKNOWLEDGMENTS

This work was supported by the European Union (European Social Fund) and the Free State of Saxony (Sächsische Aufbaubank) in the young researcher group 'InnovaSens' (SABNr. 080942409). L.R. and G.C. further acknowledge the World Class University program funded by the Ministry of Education, Science, and Technology Program through the National Research Foundation of Korea (R31-10100). This work is also funded by the German Research Foundation (DFG) within the Cluster of Excellence "Center for Advancing Electronics Dresden". D. Nozaki calculated the molecule lengths. We thank IPF Dresden for being able to measure with their Q-Sense QCM-D and zeta-potential devices. We acknowledge the support with gelelectrophoresis experiments by R. Chrétien and thank for the AFAM measurements carried out by M. Kopycinska-Müller and N. Kuzeyeva at IZFP Dresden. We thank A. Henseleit from TU Dresden for fruitful discussions. Further thanks go to V. Hintze from TU Dresden for TGF-β1 supply and to A. Hebert from TU Berlin for cooperation and carrying out the ATR-FTIR measurement.

ABBREVIATIONS

TBA1, thrombin binding aptamer 1
TBA2, thrombin binding aptamer 2
μCP, microcontact printing
QCM-D, quartz-crystal microbalance with dissipation monitoring
PBS, phosphate buffered saline
F2B, fluorescence-to-background amplification ratio

TGF-β1, recombinant human transforming growth factor beta 1
ATR-FTIR, attenuated total reflectance Fourier transform infrared spectroscopy

REFERENCES

(1) Wang, J. *Biosens. Bioelectron.* **2006**, *21*, 1887−1892.
(2) Yogeswaran, U.; Chen, S. *Sensors* **2008**, *8*, 290−313.
(3) Bidwell, D. E.; Bartlett, A.; Voller, A. *J. Infect. Dis.* **1977**, *136*, S274−S278.
(4) Ellington, A. D.; Szostak, J. W. *Nature* **1990**, *346*, 818−822.
(5) Schlecht, U.; Malave, A.; Gronewold, T.; Tewes, M.; Loehndorf, M. *Anal. Chim. Acta* **2006**, *573*, 65−68.
(6) Khati, M. *J. Clin. Pathol.* **2010**, *63*, 480−487.
(7) Liao, W.; Cui, X. T. *Biosens. Bioelectron.* **2007**, *23*, 218−224.
(8) Kim, K.; Lee, H.; Yang, J.; Jo, M.; Hahn, S. *Nanotechnology* **2009**, *20*, 235501.
(9) Lee, H.; Kim, K.; Kim, C.; Hahn, S.; Jo, M. *Biosens. Bioelectron.* **2009**, *24*, 1801−1805.
(10) An, T.; Kim, K.; Hahn, S. K.; Lim, G. *Lab Chip* **2010**, *10* (16), 2052−6.
(11) Henseleit, A.; Schmieder, S.; Bley, T.; Sonntag, F.; Schilling, N.; Quenzel, P.; Danz, N.; Klotzbach, U.; Boschke, E. *Eng. Life Sci.* **2011**, *11*, 573−579.
(12) Sassolas, A.; Blum, L. J.; Leca-Bouvier, B. D. *Biosens. Bioelectron.* **2011**, *26*, 3725−3736.
(13) Wang, X.; Ishii, Y.; Ruslinda, A. R.; Hasegawa, M.; Kawarada, H. *ACS Appl. Mater. Interfaces* **2012**, *4*, 3526−3534.
(14) Cho, E. J.; Collett, J. R.; Szafranska, A. E.; Ellington, A. D. *Anal. Chim. Acta* **2006**, *564*, 82−90.
(15) Lao, Y.-H.; Peck, K.; Chen, L.-C. *Anal. Chem.* **2009**, *81*, 1747−1754.
(16) Ray, S.; Mehta, G.; Srivastava, S. *Proteomics* **2010**, *10*, 731−748.
(17) Meneghello, A.; Sosic, A.; Antognoli, A.; Cretaio, E.; Gatto, B. *Microarrays* **2012**, *1*, 95−106.
(18) Jonkheijm, P.; Weinrich, D.; Schröder, H.; Niemeyer, C.; Waldmann, H. *Angew. Chem., Int. Ed.* **2008**, *47*, 9618−9647.
(19) Dugas, V.; Elaissari, A.; Chevalier, Y. In *Recognition Receptors in Biosensors*, 1st ed.; Zourob, M., Ed.; Springer Science +Business Media: New York, 2010; pp 47−134.
(20) Lu, B.; Smyth, M. R.; O'Kennedy, R. *The Analyst* **1996**, *121*, 29R−32R.
(21) O'Sullivan, C. K. *Anal. Bioanal. Chem.* **2002**, *372*, 44−48.
(22) Bini, A.; Minunni, M.; Tombelli, S.; Centi, S.; Mascini, M. *Anal. Chem.* **2007**, *79*, 3016−3019.
(23) Baldrich, E. In *Recognition Receptors in Biosensors*; Zourob, M., Ed., 1st ed.; Springer Science +Business Media: New York, 2010; pp 675−722.
(24) Tasset, D. M.; Kubik, M. F.; Steiner, W. *J. Mol. Biol.* **1997**, *272*, 688−698.
(25) Wu, Z.-S.; Zheng, F.; Shen, G.-L.; Yu, R.-Q. *Biomaterials* **2009**, *30*, 2950−2955.
(26) Toulmé, J. J.; Daguer, J.-P.; Dauss, E. In *Aptamers in Bioanalysis*, 1st ed.; Mascini, M., Ed.; John Wiley & Sons: Hoboken, NJ, 2009; pp 3−30.
(27) Jayasena, S. D. *Clin. Chem.* **1999**, *45*, 1628−1650.
(28) Stubbs, M. T.; Bode, W. *Thromb. Res.* **1993**, *69*, 1−58.
(29) Shuman, M. A.; Majerus, P. W. *J. Clin. Invest.* **1976**, *58*, 1249−1258.
(30) Lee, M.; Walt, D. R. *Anal. Biochem.* **2000**, *282*, 142−146.
(31) Kirby, R.; Cho, E.; Gehrke, B.; Bayer, T.; Park, Y.; Neikirk, D. P.; McDevitt , J. T.; Ellington, A. D. *Anal. Chem.* **2004**, *76*, 4066−4075.
(32) Xiao, Y.; Lubin, A. A.; Heeger, A. J.; Plaxco, K. W. *Angew. Chem., Int. Ed.* **2005**, *44*, 5456−5459.
(33) Hianik, T.; Ostatna, V.; Zajacova, Z.; Stoikova, E.; Evtugyn, G. *Bioorg. Med. Chem. Lett.* **2005**, *15*, 291−295.
(34) Lee, S. J.; Tatavarty, R.; Gu, M. B. *Biosens. Bioelectron.* **2012**, *38*, 302−307.
(35) Tennico, Y. H.; Hutanu, D.; Koesdjojo, M. T.; Bartel, C. M.; Remcho, V. T. *Anal. Chem.* **2010**, *82*, 5591−5597.
(36) Huang, H.; Zhu, J.-J. *Biosens. Bioelectron.* **2009**, *25*, 927−930.
(37) Qiu, H.; Sun, Y.; Huang, X.; Qu, Y. *Colloids Surf., B* **2010**, *79*, 304−308.
(38) Centi, S.; Tombelli, S.; Minunni, M.; Mascini, M. *Anal. Chem.* **2007**, *79*, 1466−1473.
(39) Padmanabhan, K.; Tulinsky, A. *Acta Crystallogr., Sect. D* **1996**, *52*, 272−282.
(40) Balamurugan, S.; Obubuafo, A.; McCarley, R. L.; Soper, S. A.; Spivak, D. A. *Anal. Chem.* **2008**, *80*, 9630−9634.
(41) Kumar, A.; Whitesides, G. M. *Appl. Phys. Lett.* **1993**, *63*, 2002−2004.
(42) Xia, Y.; Whitesides, G. M. *Annu. Rev. Mater. Sci.* **1998**, *28*, 153−184.
(43) Arslan, G.; Özmen, M.; Hatay, I.; Gübbük, I. H.; Ersöz, M. *Turk. J. Chem.* **2008**, *32*, 313−321.
(44) Lipomi, D. J.; Martinez, R. V.; Cademartiri, L.; Whitesides, G. M. In *Polymer Science: A Comprehensive Reference*, 1st ed.; Elsevier B.V.: Amsterdam, 2012; Vol. 7, pp 211−230.
(45) Cui, Y.; Wei, Q.; Park, H.; Lieber, C. *Science* **2001**, *293*, 1289.
(46) Kim, S.; Rim, T.; Kim, K.; Lee, U.; Baek, E.; Lee, H.; Baek, C.-K.; Meyyappan, M.; Deen, M. J.; Lee, J.-S. *The Analyst* **2011**, *136*, 5012−5016.
(47) GhoshMoulick, R.; Vu, X. T.; Gilles, S.; Mayer, D.; Offenhaeusser, A.; Ingebrandt, S. *Phys. Status Solidi A* **2009**, *206*, 417−425.
(48) Eisen, M.; Brown, P. *Methods Enzymol* **1999**, *303*, 179−205.
(49) Ember, S. W. J.; Schulze, H.; Ross, A. J.; Luby, J.; Khondoker, M.; Giraud, G.; Terry, J. G.; Ciani, I.; Tlili, C.; Crain, J.; Walton, A. J.; Mount, A. R.; Ghazal, P.; Bachmann, T. T.; Campbell, C. J. *Anal. Bioanal. Chem.* **2011**, *401*, 2549−2559.
(50) Patolsky, F.; Lieber, C. *Mater. Today* **2005**, *8*, 20−28.
(51) Huang, D.; Niu, C.; Qin, P.; Ruan, M.; Zeng, G. *Talanta* **2010**, *83*, 185−189.
(52) Sosic, A.; Meneghello, A.; Cretaio, E.; Gatto, B. *Sensors* **2011**, *11*, 9426−9441.
(53) Daniel, C.; Mélaïne, F.; Roupioz, Y.; Livache, T.; Buhot, A. *Biosens. Bioelectron.* **2013**, *40*, 186−192.
(54) Xu, Y.; Yang, L.; Ye, X.; He, P.; Fang, Y. *Electroanalysis* **2006**, *18*, 1449−1456.
(55) Jeon, N. L.; Finnie, K.; Branshaw, K.; Nuzzo, R. G. *Langmuir* **1997**, *13*, 3382−3391.
(56) Michel, O.; Ravoo, B. J. *Langmuir* **2008**, *24*, 12116−12118.
(57) Ravoo, B. J. *J. Mater. Chem.* **2009**, *19*, 8902−8906.
(58) Calabretta, A.; Wasserberg, D.; Posthuma-Trumpie, G. A.; Subramaniam, V.; van Amerongen, A.; Corradini, R.; Tedeschi, T.; Sforza, S.; Reinhoudt, D. N.; Marchelli, R.; Huskens, J.; Jonkheijm, P. *Langmuir* **2011**, *27*, 1536−1542.
(59) Rabe, U. In *Applied Scanning Probe Methods II−Scanning Probe Microscopy Techniques*, 1st ed.; Bushan, B.; Fuchs, H., Eds.; Springer-Verlag: Berlin, 2006; Vol. 2, pp 37−90.
(60) Flink, S.; van Veggel, F. C. J. M.; Reinhoudt, D. N. *J. Phys. Org. Chem.* **2001**, *14*, 407−415.
(61) Charlton, C.; Gubala, V.; Gandhiraman, R. P.; Wiechecki, J.; Le, N. C. H.; Coyle, C.; Daniels, S.; MacCraith, B. D.; Williams, D. E. *J. Colloid Interface Sci.* **2011**, *354*, 405−409.
(62) Lapin, N. A.; Chabal, Y. J. *J Phys. Chem. B* **2009**, *113*, 8776−8783.
(63) Niu, S. S.; Qu, L. L.; Zhang, Q. Q.; Lin, J. J. *Anal. Biochem.* **2012**, *421*, 6−6.
(64) Zhao, Q.; Lu, X.; Yuan, C.-G.; Li, X.-F.; Le, X. C. *Anal. Chem.* **2009**, *81*, 7484−7489.
(65) Cai, H.; Lee, T.; Hsing, I. *Sens. Actuators, B* **2006**, *114*, 433−437.